SWIPT in 3-D Bipolar Ad Hoc Networks with Sectorized Antennas

Ioannis Krikidis, *Senior Member, IEEE*

arXiv:1604.05483v1 [cs.IT] 19 Apr 2016

***Abstract*—In this letter, we study the simultaneous wireless information and power transfer (SWIPT) concept in 3-D bipolar ad hoc networks with spatial randomness. Due to three spatial dimensions of the network, we introduce a 3-D antenna sectorization that exploits the horizontal and the vertical spatial separation. The impact of 3-D antenna sectorization on SWIPT performance is evaluated for the power-splitting technique by using stochastic geometry tools. Theoretical and numerical results show that 3-D sectorization achieves a more accurate beam steering in the 3-D space, which can be beneficial for both the information and the power transfer.**

***Index Terms*—SWIPT, power-splitting, 3-D sectorized antennas, 3-D Poisson bipolar network, stochastic geometry.**

I. Introduction

SIMULTANEOUS wireless information and power transfer (SWIPT) is a new communication paradigm, where wireless devices extract information and energy from the received radio-frequency (RF) signals [1]. Due to practical limitations, SWIPT cannot be performed from the same signal without losses and practical implementations divide the received signal in two parts; one part is used for information transfer and another part is used for power transfer [2]. In this work, we focus on the power splitting (PS) technique, where the signal is split into two separate streams of different power [1], [2]. The time-splitting technique, where SWIPT is performed in the time domain, is a special case of PS with a binary power splitting parameter and therefore is excluded in our analysis.

Due to the importance of path-loss degradation on SWIPT systems, recent works study SWIPT from a large-scale point of view by taking into account the spatial randomness of the network deployment [3]. In these works, the location of the devices and/or base stations is mainly modeled as a homogeneous Poisson point process (HPPP) in the 2-D space. To further boost the information/power transfer, directivity gains through antenna sectorization is introduced as a promising technology. Sectorized antennas not only efficiently handle multi-user interference through spatial separation [4], but also facilitate wireless power transfer in environments with poor propagation characteristics [5]. However, most of the work on SWIPT with/without sectorized antennas is limited to 2-D networks and does not consider recent 3-D deployments.

A first effort to analyze the performance of a 3-D network is presented in [6], where the authors study the coverage probability for a 3-D large-scale cellular network with omni-directional antennas. On the other hand, recent standardization activities (e.g, 3GPPP) focus on full-dimension multiple-input multiple-output technology, where antenna elements are placed into a 2-D planar array in order to achieve spatial separation to both the elevation and the traditional azimuth domains [7], [8]. The employment of 3-D antenna sectorization on 3-D networks with geometric randomness is a new research area without any previous work.

In this letter, we study antenna sectorization for 3-D bipolar ad hoc networks with SWIPT-PS capabilities. Conventional 2-D sectorized models [4] are extended to capture spatial separation in the horizontal domain as well as the vertical domain. The impact of 3-D sectorized antennas on the achieved information and power transfer is evaluated by using stochastic geometry tools. Closed-form expressions as well as asymptotic simplifications are derived for the success probability and the average harvested energy. We reveal that 3-D antenna sectorization is a useful tool for 3-D networks and the associated additional degree of freedom (i.e., vertical spatial separation) achieves a higher information/power transfer than conventional antenna configurations. The main contributions of this letter are the development of a new 3-D antenna sectorization model for 3-D networks and its study in the context of SWIPT.

II. System model

We consider a 3-D Poisson bipolar ad hoc network consisting of a random number of transmitter-receiver pairs [4]. The transmitters form a HPPP $\Phi = \{x_k \in \mathbb{R}^3\}$ with $k \geq 1$ of density λ in the 3-D space [9, Sec. 2.4], where x_k denotes the coordinates of the node k. Each transmitter has a dedicated receiver (not a part of Φ) at an Euclidean distance d_0 in some random direction. The time is considered to be slotted and in each time slot all the sources are active without any coordination or scheduling process. To analyze the performance of the network, consider a typical receiver located at the origin [9]. This 3-D set-up is inline with ultra-dense urban networks, where a vast number of devices such as smartphones, tablets, sensors, connected objects will be connected in the same frequency band. These devices can be randomly spread in both the horizontal/vertical spatial domains in a chaotic manner.

We assume that wireless links suffer from both small-scale block fading and large-scale path-loss effects. The fading is Rayleigh distributed[1] so the power of the channel fading is an exponential random variable with unit variance [6]. We denote by h_x the power of the channel fading for the link between the interfering transmitter x and the typical receiver; h_0 denotes the power of the channel for the typical link. The path-loss model assumes that the received power is proportional to

I. Krikidis is with the Department of Electrical and Computer Engineering, University of Cyprus, Nicosia 1678 (E-mail: krikidis@ucy.ac.cy).

This work was supported by H2020-MSCA-RISE under Grant 690750.

[1]More sophisticated 3-D channel models that capture the spatial correlation between the horizontal and the vertical domain are beyond the scope of this letter [8].

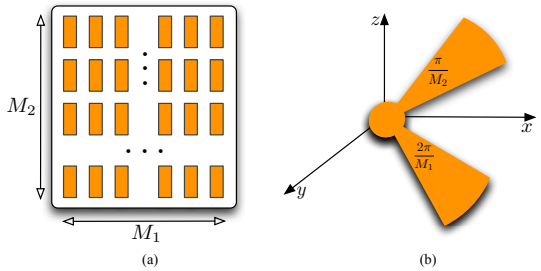

Fig. 1. a) 2-D sectorized planar antenna array with $M_1 \times M_2 = M$ elements; b) Sector size for the horizontal domain ($2\pi/M_1$) and the vertical domain (π/M_2).

$1/(1+d^{\alpha})$ where d is the Euclidean distance between the transmitter and the receiver, $\alpha > 3$ denotes the path-loss exponent[2]. In addition, all wireless links exhibit additive white Gaussian noise (AWGN) with variance σ^2.

A. Azimuth and vertical sectorization (AVS)

The transmitters are equipped with sectorized planar antenna arrays to steer their beams to specific directions in both the azimuth and the vertical domains [7], [8]. Each planar antenna array consists of $M_1 \times M_2 = M$ equally spaced antenna elements arranged in a regular rectangular array in the 2-D plane; Fig. 1 schematically shows the planar antenna array and the associated azimuth/vertical sectorization. Each antenna element covers an angle $\frac{2\pi}{M_1}$ in the horizontal domain with directivity gain M_1, and an angle $\frac{\pi}{M_2}$ in the vertical domain with associated directivity gain M_2. We also assume a constant sidelobe level γ for each antenna dimension with $0 < \gamma < 1$ without loss of generality, where γ denotes the ratio of the sidelobe level to the main lobe for the out-of-sector transmitted power for the horizontal and the vertical dimensions [4]. The receivers are equipped with a single isotropic antenna and intercept RF electromagnetic fields equally in all possible directions in 3-D space.

Due to the 3-D sectorization, three interference terms appear as follows: Φ_1 represents the set of interferers which are aligned with the location of the typical receiver in the horizontal/vertical domains; Φ_1 is a HPPP in the 3-D space with density $\lambda_1 = \lambda\frac{1}{M_1}\frac{1}{M_2} = \frac{\lambda}{M}$ (thinning operation [9]). Φ_2 is the set of interferers which are aligned with the typical receiver only in the horizontal domain; Φ_2 is a 3-D HPPP with density $\lambda_2 = \lambda\frac{1}{M_1}\frac{M_2-1}{M_2} = \lambda\frac{M_2-1}{M}$. Φ_3 refers to the set of interferers which transmit in different horizontal and vertical directions from the location of the typical receiver; it is also a 3-D HPPP with density $\lambda_3 = \lambda\frac{M_1-1}{M_1}$. We note that the vertical domain is taken into account only when the interference link is aligned with the horizontal location of the typical receiver; if an interferer occurs in a misaligned horizontal sector then its vertical sector is also misaligned.

By using similar arguments with [4], Table I summarizes the interference characteristics for each of these processes,

[2]The condition $\alpha > 3$ ensures the validity of the derived closed-form expressions and holds for practical urban/suburban wireless environments. The considered path-loss model ensures that the path-loss is always larger than one for any distance [9] and is appropriate for SWIPT systems.

TABLE I
CHARACTERISTICS OF THE INTERFERENCE PROCESSES

-	λ_i	θ_i	ϕ_i	ψ_i
I_1	$\lambda\frac{1}{M}$	$2\pi\frac{1}{M_1}$	$\pi\frac{1}{M_2}$	$\frac{M}{(1+\gamma(M_1-1))(1+\gamma(M_2-1))}$
I_2	$\lambda\frac{M_2-1}{M}$	$2\pi\frac{1}{M_1}$	$\pi\frac{M_2-1}{M_2}$	$\frac{\gamma M}{(1+\gamma(M_1-1))(1+\gamma(M_2-1))}$
I_3	$\lambda\frac{(M_1-1)}{M_1}$	$2\pi\frac{M_1-1}{M_1}$	π	$\frac{\gamma^2 M}{(1+\gamma(M_1-1))(1+\gamma(M_2-1))}$

where λ_i is the node density of the process Φ_i, θ_i and ϕ_i denote the sector size over which the process occurs for the horizontal and the vertical domain, respectively, and ψ_i is the total antenna directivity gain. As for the direct links, we assume that the transmitters are perfectly aligned with their associated receivers i.e., the antenna directivity gain equals to ψ_1.

B. SWIPT at the receivers

The transmitters have their own power supply (e.g., battery) and transmit with full power P_t. The receivers employ a SWIPT-PS technique and thus split the received signal into two flows of different power for information decoding and energy harvesting, respectively. Let $0 < \nu \leq 1$ denote the PS parameter for each receiver [2]. The energy harvesting circuit is ideal and the corresponding activation threshold is equal to zero [1], [3]. As for the information decoding process, an extra noise is introduced by the conversion operation of the RF band to baseband signal, which is modeled as AWGN with zero mean and variance σ_C^2. The signal-to-interference-plus-noise ratio (SINR) at the typical receiver can be written as

$$\mathsf{SINR} = \frac{\frac{\nu P_t \psi_1 h_0}{\eta}}{\nu[\sigma^2 + P_t(I_1+I_2+I_3)] + \sigma_C^2}, \tag{1}$$

where $\eta \triangleq 1 + d_0^{\alpha}$ and $I_i \triangleq \psi_i \sum_{x\in\Phi_i} \frac{h_x}{1+d_x^{\alpha}}$ denotes the (normalized) aggregate interference generated by the transmitters in Φ_i.

III. PERFORMANCE ANALYSIS

In this section, we study the information and power transfer performance of the 3-D bipolar ad hoc network.

A. Information transfer- success probability

The information transfer performance of the network is analyzed in terms of success probability i.e., the probability that the receiver can support a target SINR threshold β. The probability of successful transmission for the typical receiver is

$$\begin{aligned}
\Pi_{\mathsf{AVS}} &= \mathbb{P}\{\mathsf{SINR} \geq \beta\} \\
&= \mathbb{P}\left\{h_0 \geq \frac{\beta\eta[\nu(\sigma^2 + P_t\sum_{i=1}^{3} I_i) + \sigma_C^2]}{\nu\psi_1 P_t}\right\} \\
&= \exp\left(-\frac{\beta\eta(\nu\sigma^2+\sigma_C^2)}{\nu\psi_1 P_t}\right)\mathbb{E}_{\Phi}\exp\left(-\frac{\beta\eta\sum_{i=1}^{3} I_i}{\psi_1}\right) \\
&= \exp\left(-\frac{\beta\eta(\nu\sigma^2+\sigma_C^2)}{\nu\psi_1 P_t}\right)\prod_{i=1}^{3}\mathbb{E}_{\Phi_i}\exp\left(-\beta\eta I_i/\psi_1\right) \\
&= \exp\left(-\frac{\beta\eta(\nu\sigma^2+\sigma_C^2)}{\nu\psi_1 P_t}\right)\prod_{i=1}^{3}\mathcal{L}_I\left(\frac{\psi_i\beta\eta}{\psi_1}, \lambda_i\right), \qquad (2)
\end{aligned}$$

$$\Pi_{\mathsf{AVS}}^{\infty} \rightarrow \mathcal{L}_I\left(\beta\gamma^2\eta, \lambda\right) \quad \text{for } P_t, M \rightarrow \infty, \tag{3}$$

where $L_I(\cdot)$ denotes the Laplace transform of the interference and is given in the Appendix.

The performance of conventional antenna configurations yields from (2) with appropriate parameterization. Specifically, the case where the transmitters are equipped with single omni-directional antennas (case "OM") [6] refers to $M_1 = M_2 = 1$ and is equal to

$$\Pi_{\text{OM}} = \exp\left(-\frac{\beta\eta(\nu\sigma^2 + \sigma_C^2)}{\nu P_t}\right)\mathcal{L}_I(\beta\eta, \lambda), \quad (4)$$

$$\Pi_{\text{OM}}^{\infty} \to \mathcal{L}_I(\beta\eta, \lambda) \quad \text{for } P_t \to \infty. \quad (5)$$

The case where the transmitters are equipped with a 1-D linear array of M sectorized antennas for spatial separation on the traditional azimuth domain [4] (case "AS") refers to $M_1 = M$, $M_2 = 1$ and corresponds to

$$\Pi_{\text{AS}} = \exp\left(-\frac{\beta\eta(\nu\sigma^2 + \sigma_C^2)(1+\gamma(M-1))}{\nu M P_t}\right) \times \mathcal{L}_I(\beta\eta, \lambda/M)\mathcal{L}_I(\beta\gamma\eta, \lambda(M-1)/M), \quad (6)$$

$$\Pi_{\text{AS}}^{\infty} \to \mathcal{L}_I(\beta\gamma\eta, \lambda) \quad \text{for } P_t, M \to \infty. \quad (7)$$

By comparing the asymptotic expressions in (3), (5), and (7), we have $\Pi_{\text{OM}}^{\infty} < \Pi_{\text{AS}}^{\infty} < \Pi_{\text{AVS}}^{\infty}$.

B. Power transfer- average harvested energy

On the other hand, RF energy harvesting is a long term operation and is expressed in terms of average harvested energy [1]. If $100(1-\nu)\%$ of the received energy is used for rectification, the average energy harvesting at the typical receiver is expressed as

$$\begin{aligned}\mathsf{E}_{\text{AVS}} &= \zeta\mathbb{E}_{\Phi,h}(1-\nu)\left[\frac{P_t\psi_1 h_0}{\eta} + P_t(I_1+I_2+I_3)\right] \\ &= \zeta(1-\nu)P_t\left(\frac{\psi_1}{\eta} + \sum_{i=1}^{3}\psi_i\mathbb{E}_{\Phi_i}\sum_{x\in\Phi_i}\frac{1}{1+d_x^{\alpha}}\right) \\ &= \zeta(1-\nu)P_t\left(\frac{\psi_1}{\eta} + \sum_{i=1}^{3}\psi_i\mathcal{E}_I(\lambda_i)\right), \quad (8)\end{aligned}$$

$$\mathsf{E}_{\text{AVS}}^{\infty} \to \zeta(1-\nu)P_t\left(\frac{1}{\eta\gamma^2} + \frac{4\pi^2\lambda}{\alpha\sin(\frac{3\pi}{\alpha})}\right) \text{ for } M_1, M_2 \to \infty, \quad (9)$$

where $\zeta \in (0,1]$ denotes the conversion efficiency from RF signal to DC voltage [1], [3], and $\mathcal{E}_I(\cdot)$ is given in the Appendix. It is worth noting that the RF energy harvesting from the AWGN noise is considered to be negligible. The expression in (9) shows that the average harvested energy asymptotically depends on the ratio γ, while the ambient harvested energy (i.e., harvesting from the multi-user interference) is equal to the one of the OM and AS cases (see (10), (11)).

For the special cases with $M_1 = M_2 = 1$ (single omnidirectional antenna) and $M_1 = M$, $M_2 = 1$ (sectorized linear antenna array), the average harvested energy is given by

$$\mathsf{E}_{\text{OM}} = \zeta(1-\nu)P_t\left[\frac{1}{\eta} + \frac{4\pi^2\lambda}{\alpha\sin(\frac{3\pi}{\alpha})}\right], \quad (10)$$

$$\mathsf{E}_{\text{AS}} = \zeta(1-\nu)P_t\left(\frac{M}{\eta[1+\gamma(M-1)]} + \frac{4\pi^2\lambda}{\alpha\sin(\frac{3\pi}{\alpha})}\right), \quad (11)$$

$$\mathsf{E}_{\text{AS}}^{\infty} \to \zeta(1-\nu)P_t\left(\frac{1}{\eta\gamma} + \frac{4\pi^2\lambda}{\alpha\sin(\frac{3\pi}{\alpha})}\right) \text{ with } M \to \infty. \quad (12)$$

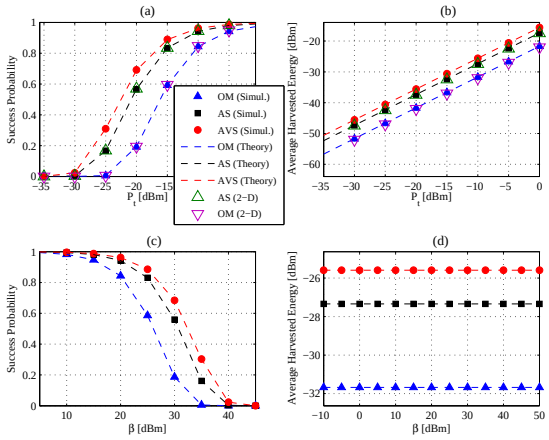

Fig. 2. a) Success probability versus P_t; b) Average harvested energy versus P_t; c) Success probability versus β; d) Average harvested energy versus β.

By comparing the asymptotic expressions in (9), (10) and (12), we have $\mathsf{E}_{\text{OM}} < \mathsf{E}_{\text{AS}}^{\infty} < \mathsf{E}_{\text{AVS}}^{\infty}$.

IV. Numerical results

Computer simulations are carried-out in order to evaluate the performance of the proposed schemes. The simulation set-up follows the description in Section II with parameters (unless otherwise defined) $P_t = -10$ dBm, $\alpha = 4$, $\lambda = 10^{-4}$, $d_0 = 3$ m, $M = 16$, $M_1 = M_2 = \sqrt{M}$, $\beta = 20$ dBm, $\sigma^2 = -130$ dBm, $\sigma_C^2 = -30$ dBm, $\nu = 0.5$, $\zeta = 1$, and $\gamma = 0.3$ [10]. Conventional antenna configurations such as omnidirectional antennas (OM) and azimuth sectorization (AS) are used as benchmarks. In addition, existing 2-D models are presented for the OM and AS configurations [6].

Fig. 2 plots the success probability and the average harvested energy versus the transmit power P_t and the SINR threshold β. As it can be seen, antenna sectorization significantly facilitates the information and the power transfer in environments with low ambient interference. 3-D sectorization achieves a more accurate beam orientation by exploiting the horizontal as well as the vertical spatial separation and thus achieves higher success probability and more efficient energy transfer by boosting the direct links. The comparison with the conventional 2-D models shows the compatibility of the 3-D models and confirms the superiority of the 3-D antenna sectorization. Theoretical curves perfectly match with the numerical results and validate our analysis.

The impact of the network density and the PS parameter on the achieved information/power transfer is depicted in Fig. 3. Fig. 3.(a) shows that sectorization is more beneficial for moderate network densities, where multi-user interference can be efficiently controlled through spatial separation. From the harvesting standpoint, Fig. 3.(b) illustrates that as λ increases, multi-user interference becomes the dominant component of the harvested energy and thus antenna sectorization has limited interest. On the other hand, Fig.'s 3.(c), 3.(d) capture the fundamental trade-off between information and energy transfer; as ν increases the success probability is improved while the harvesting process becomes less efficient, since most of the received energy is used for information decoding.

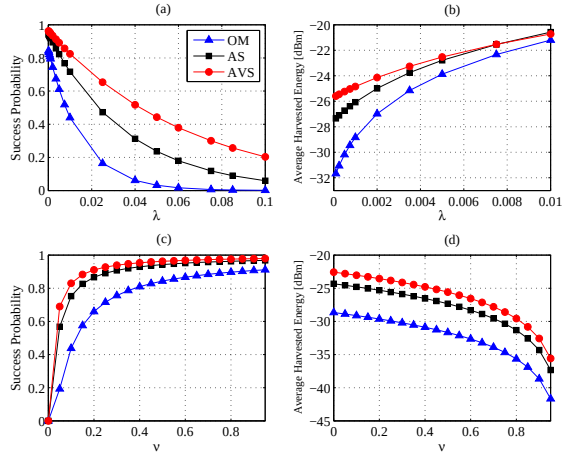

Fig. 3. a) Success probability versus λ; b) Average harvested energy versus λ; c) Success probability versus ν; d) Average harvested energy versus ν.

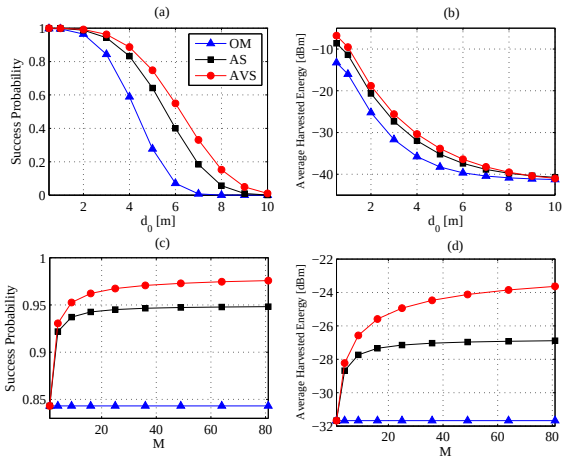

Fig. 4. a) Success probability versus d_0; b) Average harvested energy versus d_0; c) Success probability versus M; d) Average harvested energy versus M.

Finally, Fig. 4 illustrates the impact of the Euclidean distance d_0 as well as the number of antenna elements M on the system performance. As it can be seen from Fig.'s 4 (a), 4 (b), as the distance d_0 increases, the success probability decreases since the direct links become more weak. In addition, harvesting gains from antenna sectorization become less significant as d_0 increases, since the ambient multi-user interference dominates the harvesting process. Fig.'s 4 (c), 4 (d) indicate that as the number of antenna elements increases, antenna steering becomes more accurate which is beneficial for information/power transfer through direct links; the convergence floor of the curves also validates the proposed asymptotic expressions.

V. Conclusion

In this letter, a new tractable 3-D model for bipolar ad hoc networks with antenna sectorization has been presented and studied from a SWIPT point of view. Simple closed-form expressions for the success probability and the average harvested energy have been derived for the SWIPT-PS technique. Our results have shown that the 3-D antenna sectorization fully exploits the three spatial dimensions of the network and outperforms conventional antenna configurations, mainly at moderate network densities and transmitter-receiver distances.

Appendix

We derive the Laplace transform of the interference term $I = \sum_{x\in\Phi'} \frac{h_x}{1+d_x^\alpha}$, where Φ' is a thinned version of the process Φ with density $\xi \leq \lambda$. We have

$$\mathcal{L}_I(s,\xi) = \mathbb{E}_{\Phi',h} \exp(-sI) = \mathbb{E}_{\Phi',h} \prod_{x\in\Phi'} \exp\left(-\frac{sh_x}{1+d_x^\alpha}\right)$$

$$= \mathbb{E}_{\Phi'} \prod_{x\in\Phi'} \mathbb{E}_h \exp\left(-\frac{sh}{1+d_x^\alpha}\right)$$

$$= \exp\left(-4\pi\xi \int_0^\infty \left[1 - \mathbb{E}_h \exp\left(-\frac{sh}{1+r^\alpha}\right)\right] r^2 dr\right) \quad (13a)$$

$$= \exp\left(-4\pi\xi \int_0^\infty \frac{sr^2}{1+s+r^\alpha} dr\right) \quad (13b)$$

$$= \exp\left(-\frac{4\pi^2\xi}{\alpha \sin\left(\frac{3\pi}{\alpha}\right)} s(1+s)^{\frac{3-\alpha}{\alpha}}\right), \quad (13c)$$

where (13a) uses the probability generating functional of a PPP and the mapping of a 3-D PPP to one dimension (with intensity function $\xi'(r) = 4\pi\xi r^2$) [9], (13b) follows from the moment generating function of an exponential random variable i.e., $h_x \sim \exp(1)$, and (13c) is based on [11, Eq. 3.241.4].

In addition, we derive the mean interference over the HPPP Φ' as follows

$$\mathcal{E}_I(\xi) = \mathbb{E}_{\Phi',h} \sum_{x\in\Phi'} \frac{h_x}{1+d_x^\alpha} = 4\pi\xi \int_0^\infty \frac{r^2}{1+r^\alpha} dr \quad (14a)$$

$$= \frac{4\pi^2\xi}{\alpha \sin(\frac{3\pi}{\alpha})}, \quad (14b)$$

where (14a) uses the Campbell's theorem for sums [9], and (14b) is based on [11, Eq. 3.241.4].

References

[1] R. Zhang and C. K. Ho, "MIMO broadcasting for simultaneous wireless information and power transfer," *IEEE Trans. Wireless Commun.*, vol. 12, pp. 1989–2001, May 2013.

[2] I. Krikidis, S. Timotheou, S. Nikolaou, G. Zheng, D. W. K. Ng, and R. Schober, "Simultaneous wireless information and power transfer in modern communication systems," *IEEE Commun. Mag.*, vol. 52, pp. 104–110, Nov. 2014.

[3] Z. Ding and H. V. Poor, "Cooperative energy harvesting networks with spatially random users," *IEEE Sign. Proc. Lett.*, vol. 20, pp. 1211–1214, Dec. 2013.

[4] A. M. Hunter, J. G. Andrews, and S. Weber, "Transmission capacity of ad hoc networks with spatial diversity," *IEEE Trans. Wireless. Commun.*, vol. 7, pp. 5058–5071, Dec. 2008.

[5] T. A. Khan, A. Alkhateeb, and R. W. Heath, "Millimeter wave energy harvesting," *IEEE Trans. Wireless Commun.*, submitted for publication, 2015.http://arxiv.org/pdf/1509.01653v1.pdf

[6] Z. Pan and Q. Zhu, "Modeling and analysis of coverage in 3-D cellular networks," *IEEE Commun. Lett.*, vol. 19, pp. 831–834, May 2015.

[7] Y. Kim *et. al.*, "Full dimension MIMO: The next evolution of MIMO in LTE systems," *IEEE Wireless Commun.*, pp. 26–33, April 2014.

[8] J. Kang, O. Simeone, J. Kang, and S. Shamai, "Layered downlink precoding for C-RAN systems with full dimensional MIMO," *IEEE Trans. Veh. Tech.*, submitted, Nov. 2015. http://arxiv.org/pdf/1511.08084.pdf

[9] M. Haenggi, *Stochastic geometry for wireless networks*, Cambridge University Press, 2013.

[10] X. Lu, P. Wang, D. Niyato, D. I. Kim, and Z. Han, "Wireless networks with RF energy harvesting: A contemporary survey," *IEEE Commun. Surveys Tuts.*, vol. 17, pp. 757–789, 2nd Quart 2015.

[11] I. S. Gradshteyn and I. M. Ryzhik, *Table of integrals, series, and products*, Elsevier, 2007.